

# Changing eXpendable Bathythermograph Fall-rates and their Impact on Estimates of Thermosteric Sea Level Rise

Susan E Wijffels

CSIRO Marine and Atmospheric Research, Hobart, Tas., Australia

Josh Willis

Jet Propulsion Laboratory, California Institute of Technology,  
Pasadena, CA, USA

Catia M Domingues

CSIRO Marine and Atmospheric Research, Hobart, Tas., Australia

Paul Barker

CSIRO Marine and Atmospheric Research, Hobart, Tas., Australia

Neil J White

CSIRO Marine and Atmospheric Research and the Antarctic Climate  
and Ecosystem Cooperative Research Centre  
Hobart, Tas., Australia

Ann Gronell

CSIRO Marine and Atmospheric Research, Hobart, Tas., Australia

Ken Ridgway

CSIRO Marine and Atmospheric Research, Hobart, Tas., Australia

John A Church

CSIRO Marine and Atmospheric Research and the Antarctic Climate  
and Ecosystem Cooperative Research Centre  
Hobart, Tas., Australia

---

*Corresponding author address:* Susan E. Wijffels, CSIRO Marine and Atmospheric Research,  
GPO 1538, Hobart, 7000, Tas., Australia  
E-mail: Susan.Wijffels@csiro.au

## ABSTRACT

A time-varying warm bias in the global XBT data archive is demonstrated to be largely due to changes in the fall-rate of XBT probes likely associated with small manufacturing changes at the factory. Deep reaching XBTs have a different fall-rate history than shallow XBTs. Fall-rates were fastest in the early 1970s, reached a minimum between 1975-1985, reached another maximum in the late 1980s and early 1990s and have been declining since. Field XBT/CTD intercomparisons and a pseudo-profile technique based on satellite altimetry largely confirm this time-history. A global correction is presented and applied to estimates of the thermosteric component of sea level rise. The XBT fall-rate minimum from 1975-1985 appears as a 10 year 'warm period' in the global ocean in thermosteric sea level and heat content estimates using uncorrected data. Upon correction, the thermosteric sea level curve has reduced decadal variability and a larger, steadier long-term trend.

# 1. Introduction

Due to their enormous heat capacity, the oceans are absorbing most of the excess heat trapped in the climate system by the increasing concentrations of greenhouse gases. Ocean heat content can thus be used as a metric to check whether coupled climate models are correctly responding to anthropogenic and natural forcing. However, greater accuracy is needed both for global averages and on smaller scales, as regional patterns of heat content change provide important clues to changes in wind fields, changes in air-sea heat fluxes and inform how local impacts may differ from global impacts. Generating such estimates with accuracy remains a huge challenge (Levitus et al. 2005), largely due to a paucity of data in much of the global ocean, especially south of the equator. Another problem also exists – that of the changing technology used to collect ocean temperature profiles. These changes may result in technology-related biases in estimates of heat content. In the last few years, the rapidly expanding Argo array (Gould et al., 2004) is attempting to rectify many of the past problems in data quality and global coverage by delivering a truly global and highly quality controlled data stream of ocean temperature and salinity.

As the global ocean warms, its thermal expansion contributes to global sea level rise. Attempts to quantify the causes of global sea level rise – ocean thermal expansion, glacier and ice cap/sheet melting, snow-pack reduction - are confounded by the problems noted above. While the mean rates of sea level rise over the past 100 years are of great importance, decadal variability is also of interest. Church et al. (2005) show that large volcanic eruptions cool the global ocean and produce a drop in global sea levels. While this volcanic signal is clear in appropriately forced models and the global tide-gauge record, it is not as clear in the global thermosteric sea level

record (the component of sea level change due to the thermal expansion of the ocean and closely related to ocean heat content), and there are several instances where global sea level is rising but steric sea level is falling e.g. 1980-1983 (Figure 1). Can these curves be reconciled?

Gouretski and Koltermann (2007) used an ocean climatology based on the highest quality data (Nansen casts and Conductivity Temperature Depth (CTD) profiles) to compare how different instrument types measured the same ocean regions. Their study identified a clear warm bias in the abundant but low accuracy data collected by expendable bathythermographs (hereafter XBTs). This bias appears to vary from year to year. They also showed its profound impact on estimates of the time history of total ocean heat content. Here we examine the bias identified by Gouretski and Koltermann (2007 – hereafter GK) using a different method, diagnose the likely source of the error and recommend a correction.

## **2. The Fall-Rate Problem**

XBTs were developed in the early 1960s at the request of the US Navy (Seaver and Kuleshov, 1982). The instrument is essentially a thermistor embedded in the nose of an hydrodynamic bulb, with two spools of wire: one within the probe and one on the vessel which unwinds as the instrument free-falls from the surface to depth and the vessel steams away from the deployment location. The instrument collects a temperature versus time trace, with the latter converted to reported depth,  $Z_{\text{XBT}}$ , using a ‘fall rate equation’:

$$Z_{\text{XBT}} = At - Bt^2 \quad (1)$$

where  $t$  is the elapsed time in seconds since the XBT hit the ocean surface.

The bulk of XBT temperature profiles were collected using probes manufactured by Sippican Incorporated (now Lockheed Martin Sippican). Between 1965 and the late 1990s Sippican probes were produced in the USA after which their manufacture was moved to Mexico. However the Sippican probe components have remained consistent, consisting of a plastic spool with a zinc nose weight and an afterbody wrapped in plastic-coated copper wire (Sippican, personal communication). One component which has changed significantly is the XBT data system (recording mechanism), changing from analogue to digital during the 1980s.

It has long been recognised that depth determination is the most likely source of error in XBT data (Roemmich and Cornuelle, 1987). Since the mid 1970s comparison studies between simultaneous XBTs and CTDs have identified systematic errors in the computed XBT depths. Early results suggested that a small negative correction was required for the water above the thermocline while a much larger positive correction was needed for depths below it (Fedorov, 1978; Flierl and Robinson, 1977; McDowell, 1977; Seaver and Kuleshov, 1982). No official correction factor was adopted by Sippican until the early 1990s when Hanawa et al., (1995 - hereafter H95) pooled and analysed recent field intercomparisons against research-quality CTD data. Their comprehensive analysis of the field data unambiguously showed that using the manufacturer's fall rate equation resulted in deduced depths that were too shallow (and thus produced a cold temperature bias in most of the ocean). H95 recommended a new fall-rate equation for Sippican and TSK XBTs, but recommended that it not be implemented until arrangements for adequate metadata reporting about the fall-rate were put in place. As one reviewer notes '...many data providers jumped the gun and implemented the correction immediately, leading to ambiguity

(corrected/uncorrected) in data from the mid-1990s. Problems persist even to the present day since fall-rate metadata are sometimes reported incorrectly’.

It was also recommended that the reported depth for all past XBT profiles for which depth was found using the manufacturer’s original fall-rate equation should be corrected to the same effective equation by multiplying by a factor of 1.0336. Thus in the global archives of Boyer *et al.*, (2006), much work was done to provide information on which XBT profiles needed correction (supplied using old manufacturer’s fall rate equation) and which did not (i.e. those reported using the H95 fall rate equation). Despite this, and as noted above, the transition to the new fall-rate equation occurred over many years, and not all contributors have provided the necessary or correct meta-data.

### ***Data Sources and Methods***

Here we utilise temperature profiles assembled for the ENSEMBLES project by Bruce Ingleby and colleagues (Ingleby and Huddleston, 2007 – hereafter IH), and here we use the ENACT archive version 3 (hereafter EN3) which used the methods of IH and the World Ocean Data Base 5 (WOD05, Johnson *et al.*, 2006) as a data source. The archive is a composite of historical data collected in the World Ocean Database 2005 (hereafter WOD05 - Boyer *et al.*, 2006) and more recent data archived by the GTSPP project (GTSPP, 1998). IH vertically decimate the data, carry out automated QC tests and in EN3, carry along some of the necessary meta data required to distinguish profiles collected using XBTs from those collected by other platforms such as CTDs and Nansen/Niskin bottle casts (hereafter referred to as bottles).

IH also corrected XBT profiles identified in WOD05 or GTSPP as requiring correction or ‘unknown’ to the H95 fall-rate standard. However, IH modified this correction for colder regions based on the work by Thadathil *et al.* (2002) who suggested that XBT fall-rates are reduced by cold temperatures due to the increased kinematic viscosity of seawater.

To clarify and simplify our analysis, we reversed the algorithm used by IH to revert all XBT data in EN3 to the H95 standard, effectively ensuring  $f_c = 1.0336$  for all XBTs of unknown type and those identified as requiring correction (that is, those not submitted to the archives with the H95 fall-rates already applied). Thus, all XBT profiles are adjusted to the H95 fall-rate standard using the meta-data available to us.

Before XBTs came into broad-scale use in the late 1960s, the data archives are dominated by Mechanical BathyThermographs (MBTs) and bottle casts (Figure 2). Shallow XBTs initially dominate the record (almost exclusively the T4 probes manufactured by Sippican Inc. which only reach about 460m depth) while in later years deeper reaching probes (measuring to 750m and more) such as the T7 and Deep Blue dominate the XBT archive. While other XBT manufacturers exist, Lockheed Martin Sippican’s T4 and T7 probes are by far the dominant source of XBT profiles in the data base. Before the early 1990s, the meta data in the archive do not reliably allow us to distinguish whether a profile was collected using a T4 or a T7. Therefore, we have used the maximum depth of an observation to differentiate between the two kinds of probes. We designate profiles where the maximum depth is less than or equal to 550 m as ‘shallow XBTs,’ which are predominantly T4s. Observations that extend beyond 550 m are designated ‘deep XBTs’ which are predominantly T7s.

To explore the bias we first generate new global temperature climatologies for the upper 1000 m based on data from different instrument types. A local parametric fit in space and time is used following the method of Ridgway *et al.* (2002) where a 2-dimensional spatial polynomial is locally fitted to temperature on a depth surface concurrently with annual and semi-annual sinusoids at each depth. This approach can deal well with sparse data coverage as found in the Southern Hemisphere (where optimal averaging defaults to the first guess – usually a zero anomaly from a climatology), minimizes seasonal biasing and fits sharp mean ocean fronts well. However, we have extended this approach in two ways. The first is that we solve for a linear trend in time at each grid point, so that the ocean warming trend is not misdiagnosed as a platform bias (Alory, Wijffels and Meyers, 2007). The second extension is to use robust fitting methods which are less sensitive to outlier data and also provide error statistics on the fitted parameters. Here we used the method of Holland and Welsch (1977) as implemented by MATLAB® in the routine ‘robustfit’.

After some experimentation, we found that fitted parameter estimates and errors generally stabilise when 1000 or more observations are locally fit around each 1 by 1 degree grid point, suggesting this is the number required to average over eddy noise. Thus in data sparse regions the data are collected from a large spatial footprint (radius of 3 degrees in longitude, 2 degrees in latitude), which shrinks in data rich regions. Temperatures were fit on 41 depth levels, with a level every 10 m down to 150 m, 20 m down to 400 m depth and 50 m down to 1000 m depth.



Three independent temperature climatologies are generated using data from the years 1960-2005: one based on XBTs only, one based on CTDs and bottles together, and one based on MBTs only. As the fit includes a linear trend, the reference year used to compare the climatologies is 1985.

### **3. The Mean Warm Bias and its Character**

The average warm bias of XBTs identified by GK is revealed by differencing the XBT and CTD/bottle based climatologies for the year 1985 (Figure 3). At nearly all latitudes and in all ocean basins (Figure 4), we find a warm bias of between 0.05-0.3°C. The bias is small but positive ( $\sim 0.04^\circ\text{C}$ ) near the surface, is a maximum in the tropical thermocline and is more uniform below that.

One striking feature, though, is that at around 500 m, the bias drops to smaller values in deeper waters. The fact that the temperature biases have a depth dependence – small near the surface and have a maximum in the strong tropical - thermocline strongly points towards a fall-rate error. There is a consistent change in the bias around 500 m (Figure 4), the maximum depth reached by the T4 probes. This implies that shallow XBTs may have a different bias from deep XBTs. Poleward of about  $45^\circ\text{S}$  and  $55^\circ\text{N}$  the bias is less clear, and this is likely due to the larger mapping errors associated with strong fronts and currents, smaller vertical temperature gradients reducing the detectability of a depth error, and scarce data in the sub Antarctic and arctic regions. In addition, some work suggests that fall-rates are affected by ambient densities (e.g. Thadathil *et al.*, 2002), but our data might not be adequate to address this issue.

As fall-rate errors are the most likely source of biases in XBTs, the temperature errors are converted into depth reading errors using the local temperature gradient to see whether the resulting error has the right characteristics for a fall rate bias – linearly increasing with depth (Willis *et al.*, 2008). We take into account the strong seasonal cycle and secular temperature trends in the upper ocean by performing the conversion of temperature residual into a depth error estimate profile-by-profile. Thus, for each identified XBT profile, a mapped equivalent for the right year, location and season is generated using our bottle/CTD climatology. The resulting temperature residual is then converted to a depth error using the appropriate climatological temperature gradient as follows:  $dZ = dT_{\text{xbt}} / (\partial T_{\text{clim}} / \partial z)$ . Here,  $Z$  is the depth error,  $dT_{\text{xbt}}$  is the temperature residual and  $\partial T_{\text{clim}} / \partial z$  is the local climatological temperature gradient.

The individual cast depth errors, like their associated temperature residuals, are dominated by eddy variability and thus massive averaging is required to identify the small shift in the central tendency. Averaged globally and over all years the XBT depth errors do indeed show a linear dependence on depth that we argue is diagnostic of a fall rate error (Figure 5). As suggested by Figures 3 and 4, shallow XBTs have a significantly larger depth bias than deep XBTs, with depth errors of 10 m near 400 m depth compared to 5 m for deep XBTs. The averaged depth error in CTD and bottle casts is barely distinguishable from zero, which is a reassuring confirmation of the method. Near the surface estimates are noisy as the vertical temperature gradient is small there, and thus the depth error is not well defined. Interestingly, MBTs show a rough 6 m depth error with a structure that is not at all linear in depth. As we do not understand the source of this error in MBTs, we do not attempt to model and remove

it. For this reason, we recommend that MBTs be excluded from studies requiring depth accuracy of  $< 5$  m.

## **4. Time-dependency**

While it is encouraging that the XBT temperature bias appears to be caused by fall-rate errors that may be correctable, GK clearly show that this bias is not stable over time. Correction to the archive will only be possible if the data bias across the archive follows a common time history. To explore this possibility, the depth errors were averaged in different ocean basins, and also in different latitude bins. As many agencies stockpile XBTs over periods of 1-2 years (sometimes longer) our time resolution will be biennial at best, and so analyses were carried out in overlapping 2 year bins.

Remarkably, we find that a common time history does exist in the depth errors (Figure 6). For example, the diagnosed mean depth error at 600m for deep XBTs in the separate ocean basin vary together, with a minimum bias in 1985-1990 and maxima in 1978 and 2005 (Figure 6). The shallow XBTs show a similar variation but with a different magnitude of bias in the later years. Natural ocean variability does not vary uniformly in space (that is with all basins and latitudes in synchronicity) and is unlikely to vary in a way that generates a linearly increasing depth error. Therefore, the most likely source of the common time history in the depth bias of XBTs are subtle manufacturing changes at the XBT factory, which affect the fall-rates of entire batches of probes.

At the suggestion of a reviewer we checked the time-history of the bias in the northwest Pacific where large numbers of profiles were collected using XBTs manufactured by Tsurumi Seiki, Co. Ltd. (hereafter, TSK). This region does indeed feature a depth-bias time-history that is different from the other basins (Figure 6d,h), though care must be taken when averaging over a small region as ocean variability may impact the results more.

A correction is fit to the diagnosed depth biases, where the depth error is modelled as a simple multiplicative factor of depth,  $r$ , defined such that  $r = [Z_{\text{XBT}} - Z_{\text{true}}] / Z_{\text{XBT}}$ . Attempts were made to include an offset term, as well as a multiplicative factor, but the former was not stable between subsets of the archive. The fit was performed on each profile and then bin averaged. Errors are boot-strapped whereby 25% of the individual profiles in each pool are randomly sampled to produce a 50 member solution ensemble whose standard deviation is used to determine the error levels. Using a simple multiplicative factor to model depth error results in a remarkably reproducible time history between ocean basins (Figure 7), though in recent years for deep probes, we see some spread between ocean basins that might be due to incorrect meta-data about reported fall-rates.

Both types of XBTs show small biases (relative to the H95 fall-rate) in the early 1970s, just after XBTs came into widespread use. After this period, the bias grows, reaching a 6% error in the late 1970s. After this time, the error quickly returns to near zero when H95 re-examined fall-rates and set the new international standard, confirming the accuracy of the H95 results throughout the late 1980s and early 1990s. In the mid-1990s however, we see two distinct changes in the much more numerous

deep XBTs – one near 1992, and another larger change in 1999. The latter change may be associated with a shift in manufacturing site from the USA to Mexico.

The diagnosed error factors also help explain the pattern of the mean temperature bias (Figure 3). When shallow XBTs are very numerous and dominate the global archive (1972-1985) their mean depth bias is 5-6%. After 1990, deep XBTs dominate the archive with a depth bias of only 2.5%. Most of the shallow XBTs deployed globally have a large depth bias, while most deep XBTs had a depth bias roughly half as large. Thus, over the entire archive, temperatures below 500 m have a smaller warm bias than those above. Depth errors,  $r$ , diagnosed from EN3 are reported in Table 1 such that:

$$Z_{\text{true}} = Z_{\text{XBT}}(1 - r) \quad (2)$$

## 5. Comparisons with Independent Methods

Given the complexities and uncertainties of how XBT data are collected (recorder type, ship speed, probe source) and archived (accurate meta-data for probe-type and fall-rate) the derivation of a global correction based simply on year of deployment and depth of measurement would appear naive. Attempting to retrieve the correct meta-data to attack this problem in more detail far into the past archive is a very daunting task and it is likely impossible to achieve 100% accuracy. However, the fall-rate changes we have diagnosed since the early 1990s can indeed be independently checked. Based on H95's recommendations, greatly improved meta-data was collected for a larger portion of profiles sent to the global archives from the early 1990s onward. In addition the XBT data can be checked against independent

contemporaneous data – either *in situ* CTD data or altimetric satellite data. Here we use these methods to check our depth error estimates.

*a. Altimetric Pseudo-temperature Method*

Another powerful technique for characterizing the XBT bias is analysis of nearby XBT/CTD pairs as described in Willis *et al.* (2008). The technique is limited by the number of nearby XBT/CTD pairs. Since the early 1990s, however, satellite altimeters have provided global measurements of sea surface height (SSH) variability with excellent spatial and temporal resolution. A number of studies (e.g., Gilson *et al.*, 1998 and Willis *et al.*, 2004) have shown that SSH anomalies are strongly correlated with upper ocean temperature variability. By exploiting this correlation along with improved meta-data since the early 1990s, it is possible to use the altimeter data to characterize recent XBT biases in much greater detail than for earlier periods.

The “Upd” product containing gridded SSH anomalies from AVISO were used for this analysis. This product contains data from several satellite altimeters and includes variability on scales as small as ten days and 150 – 200 km (Ducet *et al.*, 2000).

For this part of the analysis, CTD data were obtained directly from both the GTSP and WOD05 databases, and Argo profile data were obtained from the Argo array of profiling floats (Gould *et al.*, 2004). XBT data were obtained from GTSP, and as above, all recommendations about application of the H95 depth correction were followed and probes of unknown type (GTSP \$DPC code 03) also had the H95 correction applied. Data quality flags provided by GTSP were used to eliminate spurious profiles when available. In addition, a 6 standard deviation test was

performed using profiles in approximate  $10^\circ \times 10^\circ$ , geographically similar boxes to eliminate additional gross outliers.

In order to use the SSH data to test for biases in XBT profiles, local, linear regression coefficients were computed between SSH and subsurface temperatures using temperature profiles from CTDs and Argo floats. Argo profiles with spurious pressure values identified by Willis *et al.* (2008) were excluded from this calculation. The regression coefficients allow subsurface temperature anomalies to be estimated from SSH anomalies as follows:

$$T_{\text{pseudo}}(z) = \alpha(x,y,z) * \text{SSH}(x,y,t), \quad (3)$$

where,  $\alpha(x,y,z)$  is local regression coefficient and  $T_{\text{pseudo}}$  is the estimate of subsurface temperature anomaly, referred to as the “pseudo-temperature” profile.

Regression coefficients were computed in  $2^\circ$  longitude x  $1^\circ$  latitude bins on each 10 m level depth from the surface to 750 m. Temperature anomalies were computed relative to the WOCE Gridded Hydrographic Climatology (WGHC, Gouretski and Koltermann, 2004). Figure 8 shows the correlation coefficient,  $r$ , between SSH and temperature anomaly at 400 m. Note that in most regions,  $r$  is greater than 0.5.

Once the regression coefficients were computed, pseudo-temperature profiles were estimated at the times and locations of all profiles from 1993 through the end of 2006. These “pseudo-pairs” were then used to examine the dependence of the XBT fall-rate bias by probe type and manufacturer. The depth error was then estimated by differencing the observed temperature and the pseudo-temperature and normalizing by

$\partial T_{\text{clim}}/\partial z$  as described above. However, for the pseudo-pair analysis the WGHC climatology was used to compute  $\partial T_{\text{clim}}/\partial z$  rather than the bottle/CTD climatology.

The pseudo-pair technique was first tested for consistency by estimating the depth error for CTD and Argo profiles. Figure 9 shows the median depth difference between CTD profiles and their pseudo-temperature pairs, grouped in 1 year increments from 1993 through 2002. With only a few thousand pairs per year, the depth differences range from 3 to 5 m. Nevertheless, the lack of any time dependence and the proximity to zero suggest that the altimeter data provides a stable, accurate tool for determining depth errors during the altimeter record.

Also shown in Figure 9 is a pseudo-pair analysis of Argo data by float type. This serves primarily as a consistency check of the technique as the floats provide most of the data used to determine the regression coefficients,  $\alpha(x,y,z)$ . Apart from the known bias in a number of SOLO floats from Woods Hole Oceanographic Institution (Willis *et al.*, 2008), most float types have profiles with nearly zero depth error relative to the pseudo-pairs, as expected. The Provor and APEX floats with FSI sensors do show slight offsets below 300 m, but with only 6000 and 1200 pseudo-pairs, respectively, there are too few of these profiles to determine whether these small offsets are significant.

The pseudo-pair technique provides an independent estimate of temperature anomaly for each individual profile. However, the altimeter data still do not resolve eddy or internal wave variability on scales smaller than about 150 km and 10 days time. For this reason, significant averaging is still necessary to produce a robust estimate of



XBT data errors. Nevertheless, this technique requires fewer pairs than a direct comparison between XBT profiles with nearby CTD and Argo profiles. This is illustrated in Figure 10, which shows the frequency distribution versus depth of the pair analysis for Sippican Deep blue XBT probe with H95 coefficients (WMO code, 052) compared with nearby Argo profiles, over the three year period from January 1, 2004, through December 31, 2006. Argo profiles were considered to be ‘nearby’ if they fell within 4 degrees longitude, 2 degrees latitude and 90 days of an XBT probe. About 14,000 such pairs were available during this period. The median value and one standard deviation range are highlighted. The frequency distribution of depth errors based on the pseudo-pair analysis for the same XBT probes is also shown in Figure 10. Note that the median value is almost identical. However, the large time and space window needed to capture a sufficient number of Argo/XBT pairs results in a larger standard deviation for that technique. For the pseudo-pair technique, the altimeter data are interpolated to the time and location of the XBT profile, resulting in a one standard deviation range that is about 12 m smaller. This suggests that fewer pairs are needed for the pseudo-pair analysis technique to converge.

Figure 11 shows the temporal evolution of the depth bias in Sippican Deep Blue XBT probe with manufacturers original fall rate coefficients (WMO 1770 code, 051) for each year from 1993 through 2005, based on the pseudo-pair analysis. About 30,000 of these probes were deployed over the entire period, and were more abundant during the 1990s. Note the sharp increase in the bias after 1999, again possibly reflecting changes in manufacturing that occurred after relocation of the main Sippican manufacturing facilities to Mexico.

Table 2 contains the temporal evolution of the depth biases of all probe types of substantial abundance in the GTSPP database computed using the pseudo-pair technique. As above, the depth error is modelled as a multiplicative factor of depth. Table 2 shows depth error,  $r$ , for each probe type and time period. Where there are fewer than 200 probes of a given type in a year, an analysis was not made. The error in  $r$  is also computed using the same bootstrap method described above. In general, the pseudo-pair method confirms the results found in the EN3 analysis (Figure 12). In particular, the step-like increase in bias among deep XBT probes is confirmed for the abundant Deep Blue probes and the shallow probes. However, for the probes identified as T7s (Figure 12b), there is marked divergence from the EN3 correction in certain years and the amplitude is close to that expected if probes are either uncorrected or double corrected with the depth factor 1.0336 suggested by H95. This illustrates a possibly serious problem with the meta-data in the archives not being consistent with the fall-rates used to determine depth.

It is important to note that the description of XBT biases presented in Table 2 may represent changes in data processing as well as any actual changes in instrument manufacture. In many profiles, ambiguities remain about which fall rate equations were used when the data were submitted to the archives. In the present analysis, we have chosen to adopt the recommendations of GTSPP over whether or not to apply the H95 depth correction factor. However, further refinement of the bias estimate may be possible by considering additional meta-data associated with the XBT profiles such as cruise number, data source or profile history. With a more precise classification of XBT probe type and fall rate equation, bias in these instruments could be better characterized and minimized.

### *b. Historical and Recent In Situ Field Comparisons*

It is also possible to compare the EN3-based history of fall-rate changes with past field assessments. To do this we convert our slope error into an estimate of the first term, A, in the XBT depth equation (1). The variability in the second order coefficient B has a much weaker affect on depth estimates than changes in the first order term A.

If  $Z_{\text{true}} = A_{\text{true}}t - Bt^2$ , and  $Z_{\text{XBT}} = A_{\text{XBT}}t - Bt^2$ , where ‘true’ is the actual fall-rate parameters, and ‘XBT’ refers to that used in EN3 (the H95 values) then ignoring the small changes in B we can estimate the implied changes in the A term via

$$A_{\text{true}} = A_{\text{XBT}}(1-r)$$

In addition to the field comparisons compiled by H95 in their Table 1, we also examine the additional *in situ* depth bias estimates listed in Table 3 where depth displacements are converted to an estimate of the A term using the reasoning above.

An *in situ* CTD/XBT comparison was also carried out in 2001 in the Tasman and Coral Seas. During a high spatial-resolution CTD section, XBTs were dropped during each CTD cast providing a direct cast-by-cast comparison. The results show a clear warm-bias in the XBT data (Figure 13) and when converted to a depth error translates to a 3% over-estimation of depth, agreeing with our analysis from EN3.

The deduced time history of the fall-rate coefficient A for deep XBTs (Figure 14), based on EN3 agrees very well with most of the published results in the literature where fall rates were actually calculated – the values from H95 Table 1 (numbered), T98 and SGB07. Ironically, the H95 assessment was done at a time when fall-rates

were faster than at any other time. The reduction of deep XBTs fall-rates since 1990 is independently confirmed by field intercomparisons (e.g. SGB07), as are the low values in the later 1970s. Before 1975 our estimate does not agree well with the depth errors in the literature, but at this time the number of deep XBTs in the data base is quite small. The comprehensive study by RBM07 also disagrees with SGB07's and our results for recent years. However, in their fitting of fall-rate parameters to the *in situ* data, they did not allow for the low values of  $A$  found by SGB07, and interestingly found a residual warm bias in their fall-rate corrected temperature values. These recent studies raise serious questions, not just about the constancy of the fall-rate equation, but also around its form.

## 6. Summary and Discussion

An analysis of temperature and implied depth errors of the XBT profiles in EN3 confirm GK07's findings that there is a time-variable warm bias in the XBT data. Here, we show that this bias is largely due to year-to-year changes in XBT fall-rates and that shallow XBTs (T4s) have a different error from deep XBTs (T7s and Deep Blues). We believe it is highly likely these are due to small changes in the manufacture of XBT probes, since the changes are to first order spatially synchronised, have the vertical characteristics of a fall-rate error, and are hard to explain in any other way. Our results are largely supported by historical and recent field intercomparisons between XBTs and CTDs, as well as a pseudo-profile technique based on satellite altimetry.

The XBT depth errors can be well modelled as a factor of total reported depth, and we present correction factors for the EN3 data up to 2005 (Table 1). It is crucial to note

that these factors apply to XBT profiles which have been adjusted to the H95 fall-rate equation. Also, we do not assert that the suggested corrections account for all the bias errors in the archive across all contributing institutions, recorder and probe-type combinations. Untangling this problem is extremely daunting, given the small amount of meta-data for pre-1990 profiles. Our results do suggest, encouragingly, that the bulk of the bias is common across these variations, and thus can be removed to first order. A more careful analysis using more of the available meta-data is warranted, and it may be particularly worthwhile revisiting historical XBT/CTD intercomparison data sets to check the form and changing coefficients of the fall-rate equation. SGB07 find a depth offset term in their data set and our Coral Sea data support this. RBM07 find a residual temperature bias. This should also be further studied. In, addition, if XBT data are to be combined in analyses with other data types, some kind of on-going batch calibration will be necessary, based either on annual field intercomparisons or using the pseudo-pair method discussed above. These issues present quite a challenge to the community.

Due to the fact that XBT profiles make up more than 70% of the global temperature profile archive, the impact of these errors on estimates of global ocean heat content changes is large as shown by GK. Using the spatial interpolation method of Church *et al.* (2004), and an unbiased XBT/CTD/bottle climatology as a reference, we estimate global ocean thermosteric sea level changes for the upper 700 m (Figure 15). When corrected for the XBT bias, thermosteric sea level (and the associated ocean heat content) shows much weaker decadal variability in the 1970s and a higher rate of rise for 1961 to 2003 (e.g. compare the fitted linear trends). Though the end-point values are similar, as found in GK the bias in the XBT data account for a large part of the

1970s decadal change in ocean heat content reported by Levitus *et al.* (2005). Based on the XBT bias corrections proposed here, Domingues *et al.* (2008) show that the average heat uptake in the upper 700 m of the ocean, from 1961 to 2003, accounts for a larger portion of sea level rise than previously believed. Their ocean warming and thermal expansion rates are about 50% larger than equivalent rates of earlier estimates (Antonov *et al.*, 2005; Levitus *et al.*, 2005; Ishii *et al.*, 2006).

*Acknowledgments.*

We thank Bruce Ingleby and the EN3 team for prompt help accessing their data set and providing enhanced meta-data to us. Suggestions by Bruce and two anonymous reviewers also improved this manuscript. This paper is a contribution to the CSIRO Climate Change Research Program and the CSIRO Wealth from Oceans Flagship and was supported by the Australian Government's Cooperative Research Centres Programme through the Antarctic Climate and Ecosystems Cooperative Research Centre. SEW, CMD, PAB, NJW, AG, KR and JAC were partly funded by the Australian Climate Change Science Program.

## References

- Alory, G., S. Wijffels, G. M. Meyers, 2007: Observed temperature trends in the Indian Ocean over 1960-1999 and associated mechanisms. *Geophys. Res. Lett.*, **34**, L02606 doi:10.1029/2006GL028044.
- Antonov, J. I., Levitus, S. & Boyer, T.P., 2005: Thermosteric sea level rise, 1955-2003. *Geophys. Res. Lett.*, **32**, L12602, doi:10.1029/2005GL023112.
- Boyer, T. P., J. I. Antonov, H. E. Garcia, D.R. Johnson, R. A. Locarnini, A.V. Mishonov, M. T. Pitcher, O. K. Baranova, I. V. Smolyar, 2006: World Ocean Database 2005, . S. Levitus, Ed., NOAA Atlas NESDIS 60, U.S. Government Printing Office, Washington, D.C., 190 pp.
- Church, J. A., N. J. White, and J. M. Arblaster, 2005: Significant decadal-scale impact of volcanic eruptions on sea level and ocean heat content, *Nature*, **438**, 74–77.
- Church, J.A, N. J. White, R. Coleman, K. Lambeck and J. X. Mitrovica, 2004: Estimates of the regional distribution of sea level rise over the 1950-2000 period. *J. Climate*, **17** (13): 2609-2625.
- Domingues, C.M., J.A. Church, N.J. White, P.J. Gleckler, S.E. Wijffels, P.M. Barker, J.R. Dunn, 2008: Improved ocean-warming estimates: implications for climate models and sea-level rise. Submitted to *Nature* (In review).

Ducet, N., P.-Y. Le Traon, G. Reverdin, 2000: Global high-resolution mapping of ocean circulation from TOPEX/Poseidon and ERS-1 and -2. *J. Geophys. Res.*, **105**, 19,477-19,498.

Fedorov, K. N., A. I. Ginzburg, and A. G. Zatsepin, 1978: Systematic differences in isotherm depths derived from XBT and CTD data. *POLYMODE News*, **50**(1), 6–7.

Flierl, G. and A. R. Robinson, 1977: XBT measurements of the thermal gradient in the MODE eddy, *J. Phys. Oceanogr.*, **7**, 300–302.

Gilson, J., D. Roemmich, B. Cornuelle, and L.-L. Fu., 1998: Relationship of TOPEX/Poseidon altimetric height to steric height and circulation of the North Pacific, *J. Geophys. Res.*, **103**, 27,947–27,965.

Global Temperature-Salinity Profile Programme, 1998: *IOC Technical Series*, **49**, UNESCO (English).

Gould, J., and the Argo Science Team, 2004: Argo Profiling Floats Bring New Era of In Situ Ocean Observations. *EoS*, Transactions of the American Geophysical Union, **85**(19).

Gouretski, V. V., and K. P. Koltermann, 2004: WOCE global hydrographic climatology [CD-ROM], Ber. Bundesamt Seeschifffahrt Hydrogr. Rep., 35, 52 pp., Bundesamt Seeschifffahrt Hydrogr., Hamburg, Germany.



Gouretski, V. V., and K. P. Koltermann, 2007: How much is the ocean really warming? *Geophys. Res. Lett.*, **34**, L01610, doi:10.1029/2006GL027834.

Hanawa, K., P. Rual, R. Bailey, A. Sy, and M. Szabados, 1995: A new depth-time equation for Sippican or TSK T-7, T-6 and T-4 expendable bathythermographs (XBT), *Deep Sea Res. I*, **42**, 1423– 1451.

Holland, P. W., and R. E. Welsch, 1977: Robust Regression Using Iteratively Reweighted Least-Squares. *Comm. in Statistics: Theory and Methods*, **A6**, 813-827.

Ingleby, B., and M. Huddleston, 2007: Quality control of ocean temperature and salinity profiles - historical and real-time data. *J. of Marine Systems*, **65**, 158-175, 10.1016/j.jmarsys.2005.11.019

Ishii, M., Kimoto, M., Sakamoto, K. & Iwasaki, S.-I., 2006: Steric sea level changes estimated from historical ocean subsurface temperature and salinity analyses. *J. Oceanogr.*, **62**, 155-170.

Johnson, D.R., T.P. Boyer, H.E. Garcia, R.A. Locarnini, A.V. Mishonov, M.T. Pitcher, O.K. Baranova, J.I. Antonov, and I.V. Smolyar, 2006: World Ocean Database 2005 Documentation. Ed. Sydney Levitus. *NODC Internal Report 18*, U.S. Government Printing Office, Washington, D.C., 163 pp,

Levitus S., J. Antonov, T. Boyer, 2005: Warming of the world ocean, 1955–2003. *Geophys. Res. Lett.*, **32**, L02604, doi:10.1029/2004GL021592.

McDowell, S., 1977: A note on XBT accuracy. *POLYMODE News*, **29**(1), 4–8.

Reseghetti, F., M. Borghini and G. M. R. Manzella, 2007: Factors affecting the quality of XBT data – results of analyses on profiles from the Western Mediterranean Sea. *Ocean Science*, **3**, 59-75.

Ridgway, K. R., J. R. Dunn, and J. L. Wilkin, 2002: Ocean interpolation by four-dimensional weighted least squares—Application to the waters around Australasia, J. *Atmos. Oceanic Technol.*, **19**(9), 1357– 1375.

Roemmich, D. and B. Cornuelle, 1987: Digitization and calibration of the expendable bathythermograph, *Deep-Sea Res.*, **34**, 299–307.

Seaver, G. A. and S. Kuleshov, 1982: Experimental and analytical error of Expendable bathythermograph. *J. Phys. Oceanogr.*, **12**, 592– 600.

Snowden, D., G. Goni and M. Baringer, 2007: A Comparison of Six Expendable Bathythermograph Data Acquisition Systems, AOML draft report.

Thadathil, P., A. K. Saran, V. V. Gopalakrishna, P Vethamony, N. Araligidad and R. Bailey, 2002: XBT fall rate in waters of extreme temperature: a case study in the Antarctic Ocean, *J. Atmos. Oceanic Technol.*, **19**, 391–396.

Willis, J. K., D. Roemmich and B. Cornuelle, 2004: Interannual variability in upper ocean heat content, temperature, and thermosteric expansion on global scales. *J. Geophys. Res.*, **109**, C12036, doi:10.1029/2003JC002260.

Willis, J. K., J. M. Lyman, G. C. Johnson, J. Gilson, 2008: In Situ Data Biases and Recent Ocean Heat Content Variability, *J. Atmos. Oceanic Technol.*, (In Review).

## List of Figures

FIG. 1 Global mean sea level (black) and an estimate of the thermosteric component (WOA, red) in the upper 700 m based on the gridded temperature data and reference climatology used in Antonov *et al.* (2005) and Levitus *et al.* (2005). Note that these time series have an *ad hoc* reference and were smoothed by a 3-year running mean.

FIG. 2. Thousands of profiles a) per year by platform in the ENACT3 archive and b) in 2.5° latitude bins, by platform type. See text for definitions of shallow and deep XBTs.

FIG. 3. Zonally-averaged temperature difference between a climatology based on XBT data alone and one based on CTD and bottle casts. The zero contour is dashed in black, and the 0.1°C contours are shown in white.

FIG. 4. Global and basin-averaged temperature difference between a climatology based on XBT data alone and one based on CTD and bottle casts for the global ocean.

FIG. 5. Global and basin-averaged depth errors across all years diagnosed from individual profile data using temperature residuals from a climatology based on CTD and bottle casts for the global ocean and the years 1969 – 2005. The thickness of the curves is the standard error around the mean of the estimates, assuming every profile is independent. This latter assumption is likely optimistic and the true error may be at least twice as large as shown.

FIG. 6. Depth error time history for each ocean basin analyzed independently. Depth errors were averaged in 2 year bins and in each ocean basin. (a) – (c) for shallow XBTs in the Indian, Pacific and Atlantic Oceans; d) shallow XBT depth error at 400 m for each basin with the Indian, Pacific and Atlantic Oceans in cyan, blue and green respectively, with the northwest Pacific (longitudes  $< 155^{\circ}\text{E}$ , latitudes  $> 25^{\circ}\text{N}$ ) in gray; (e) – (g) for deep XBTs in the Indian, Pacific and Atlantic Oceans; h) deep XBT depth error at 600 m for each basin with colours as in (d). In (d) and (h), curve thicknesses indicate the standard error of the estimate.

FIG. 7. Number of observations in 2 year bins for deep (a) and shallow (b) XBTs. XBT depth correction factor,  $r$ , averaged in overlapping 2 year bins for deep (c) and shallow (d) reaching profiles. Observation number (a, b) and fits (c, d) were analyzed in each ocean basin independently, as well as globally (see legend). Errors shown are 3 times the standard error, which encompasses 99.8% of the distribution (see text).

FIG. 8. Correlation coefficient between SSH and temperature anomaly at 400 m.

FIG. 9. Median depth error computed by comparing actual CTD profiles and their “pseudo-pairs” (left panel). Number of profiles ranges from 2000 to 6000 CTD profiles in a given year. Same for Argo float profiles by float type (right panel).

FIG. 10. Frequency distribution of difference in isotherm displacement v. depth for Sippican Deep blue XBT probe with H95 fall rate coefficients (WMO code, 052) compared with nearby Argo profiles (left panel) and pseudo pairs (right panel).

Average is over the three-year period from Jan. 1, 2004, through Dec. 31, 2006. White lines show the median and one standard deviation.

FIG. 11. Evolution of bias in for Sippican Deep blue XBT probe with old fall rate coefficients (WMO code, 051) using pseudo-pairs. The blue line shows the number of profiles used in a given year.

FIG. 12. In colours – the evolution of depth bias and its associated error (at 99% significance level) by probe type and depth equation used, as reported in Table 2. Results for shallow XBT profiles in (a) and for deep XBT profiles in (b). In the legend, T-7, T-4 and T-DB refer to Lockheed Martin Sippican's probe models identified by the WMO number in the profile meta data in the archive, with H95 and S65 indicating the reported fall-rate equation used, where H95 refers to the Hanawa et al. (1995) recommendations and S65 indicates the manufacturers original estimate. The black line is the global bias estimated from EN3 with error bars as detailed in Table 1. The two straight reference lines indicate fall-rates equal the H95 value (at zero) and the S65 value (at 0.0366).

FIG. 13. During voyage of RV Franklin (July 2001) XBT casts were made concurrently at 52 CTD locations between Fiji and Brisbane. (a) Location of CTD stations, (b) Difference in isotherm depth between XBT and CTD temperature casts. Blank areas show mixed layer and location of topography. (c) Mean difference in isotherm depth for XBT and CTD casts.

FIG. 14. Time history of the primary coefficient in the XBT fall-rate equation for deep XBTs as estimated from our analysis of the XBTs in the EN3 data set (grey line), estimates collated in H95's Table 1, and published results in Table 1 of this study. S65 refers to the manufacturer's recommended coefficient (also marked by the reference line), 'Coral01' refers to an estimate based on an XBT/CTD field comparison carried out in the Coral Sea in 2001. Text symbols are centered on the time and value they represent.

FIG. 15. Global mean thermosteric sea level estimates for the upper 700 m, relative to 1961. EN3 data, with (black) and without (blue) XBT profiles corrected for the fall-rate bias, referenced to an unbiased climatology (see text for details). WOA estimates (red) based on the data and reference climatology used in Antonov et al. (2005) and Levitus et al. (2005). Note that, in this latter case, both data and the climatology contain XBT bias. The thin straight lines are least-squares linear fits to the estimates. All time series were smoothed by a 3-year running mean.

## List of Figures

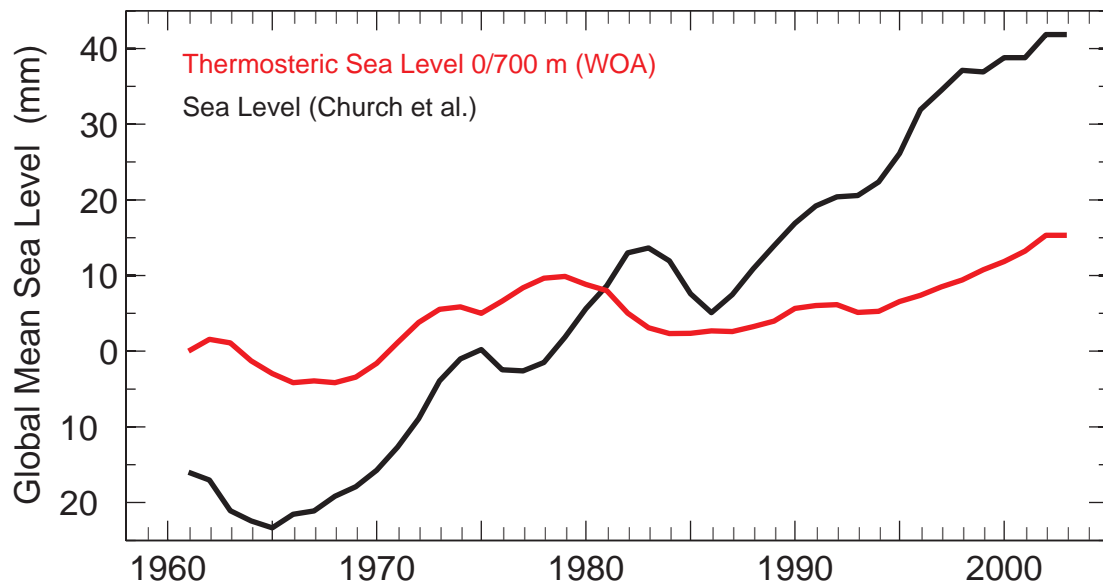


FIG. 1. Global mean sea level (black) and an estimate of the thermosteric component (WOA, red) in the upper 700 m based on the gridded temperature data and reference climatology used in Antonov *et al.* (2005) and Levitus *et al.* (2005). Note that these time series have an *ad hoc* reference and were smoothed by a 3-year running mean.



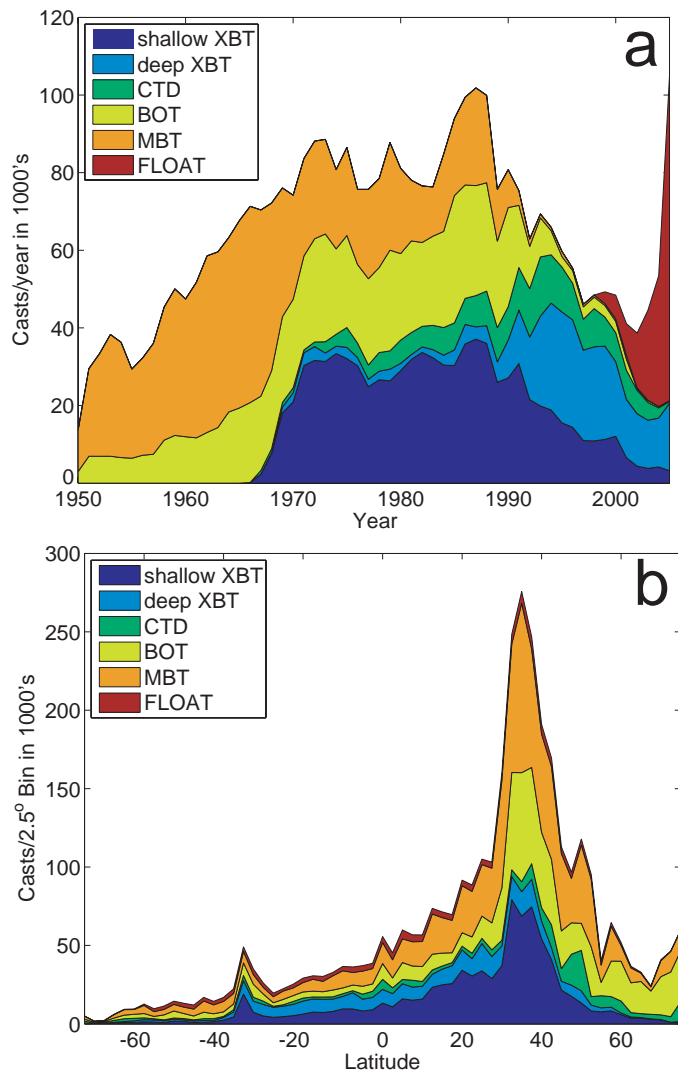


FIG. 2. Thousands of profiles a) per year by platform in the ENACT3 archive and b) in 2.5° latitude bins, by platform type. See text for definitions of shallow and deep XBTs.

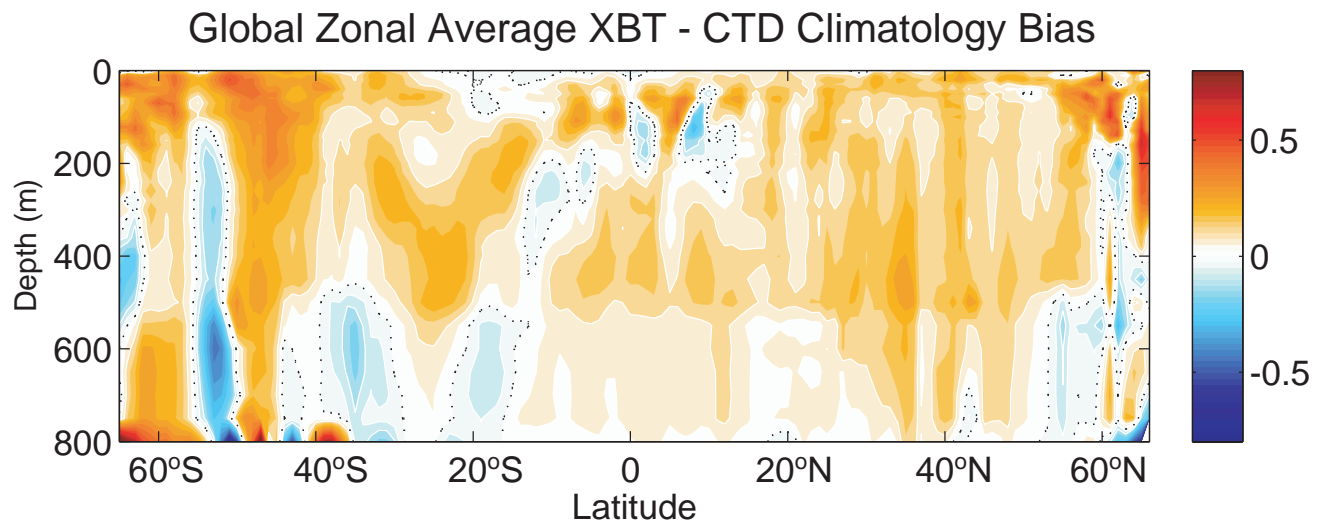


FIG. 3. Zonally-averaged temperature difference between a climatology based on XBT data alone and one based on CTD and bottle casts. The zero contour is dashed in black, and the 0.1°C contours are shown in white.

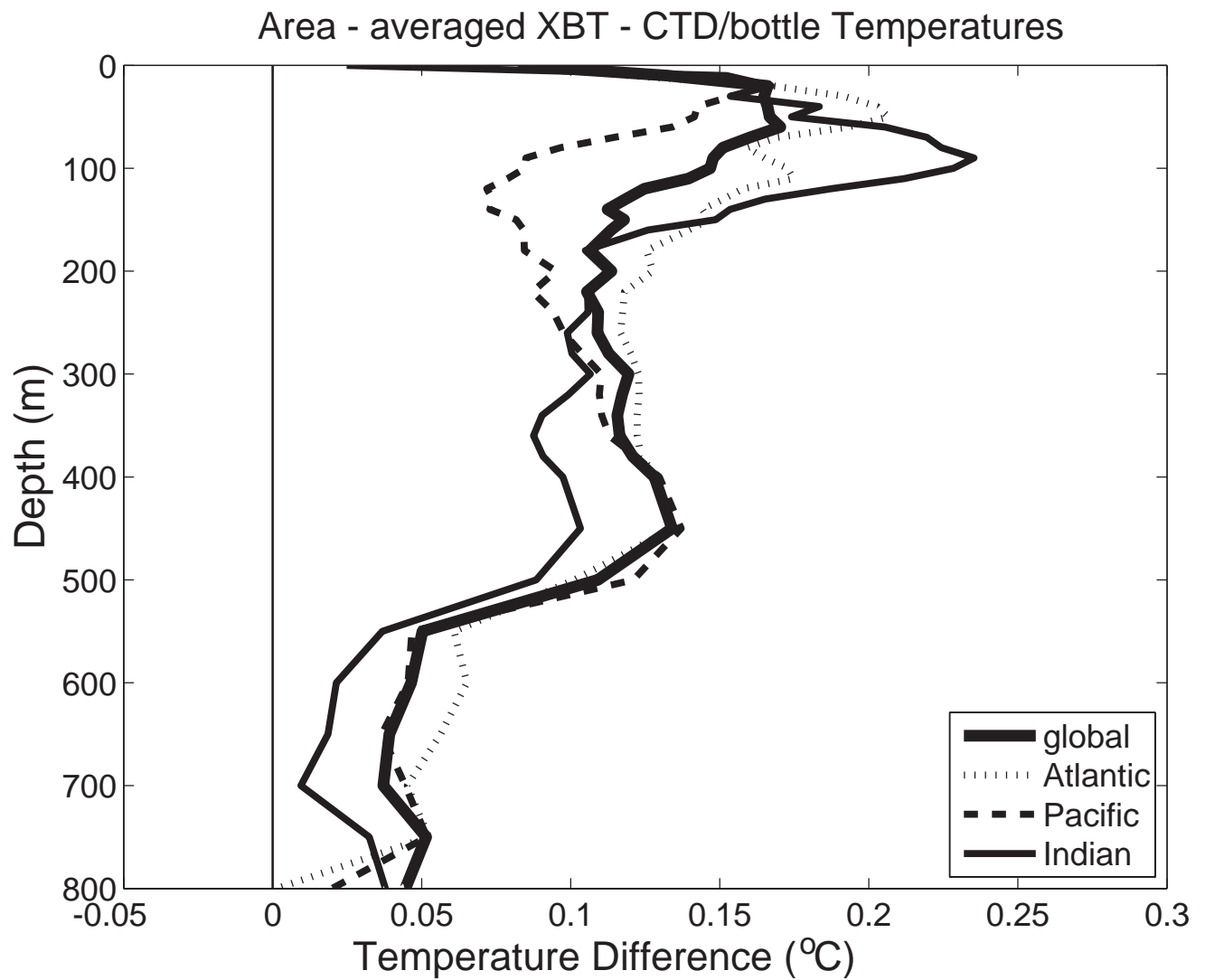


FIG. 4. Global and basin-averaged temperature difference between a climatology based on XBT data alone and one based on CTD and bottle casts for the global ocean.

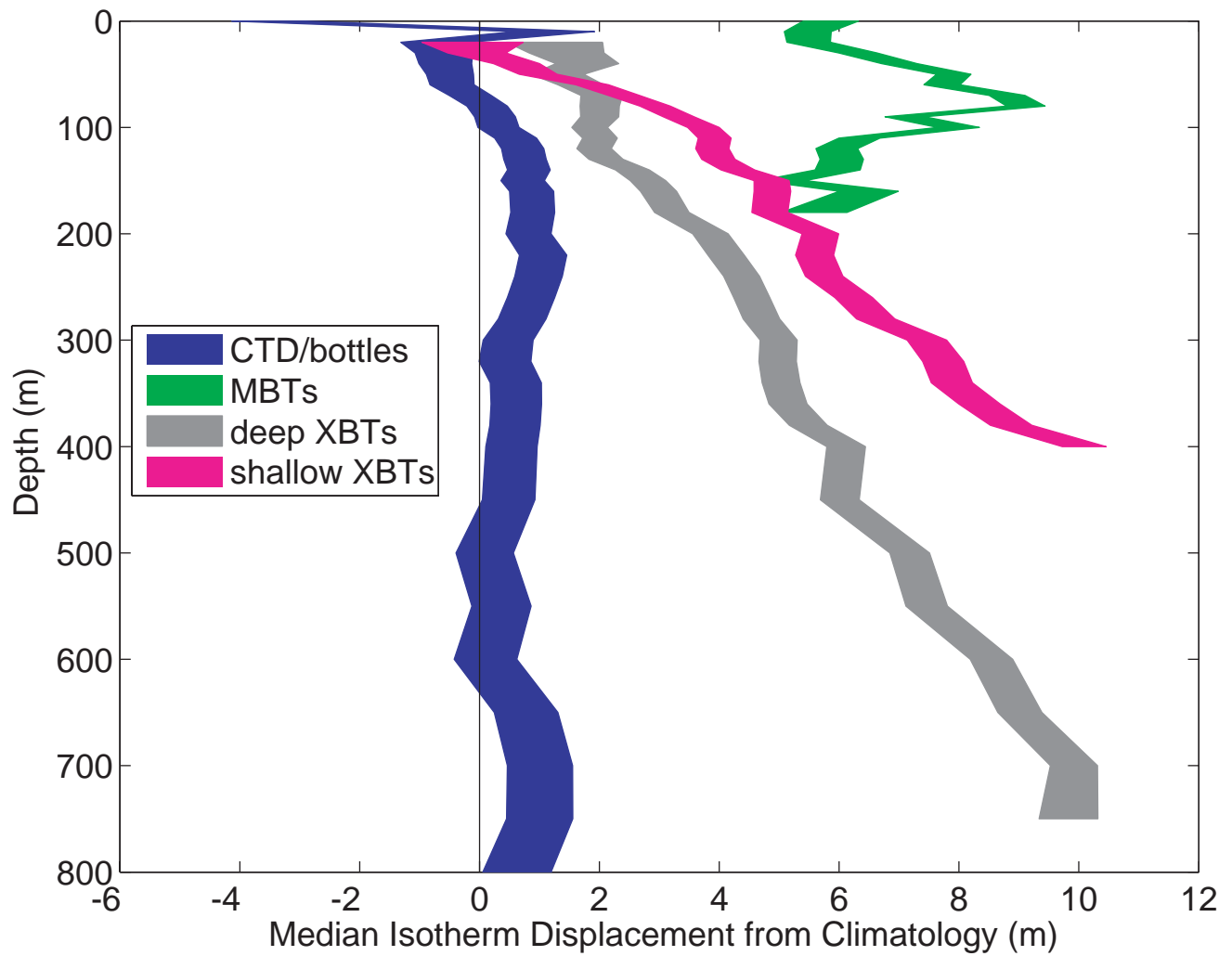


FIG. 5. Global and basin-averaged depth errors across all years diagnosed from individual profile data using temperature residuals from a climatology based on CTD and bottle casts for the global ocean and the years 1969 – 2005. The thickness of the curves is the standard error around the mean of the estimates, assuming every profile is independent. This latter assumption is likely optimistic and the true error may be at least twice as large as shown.

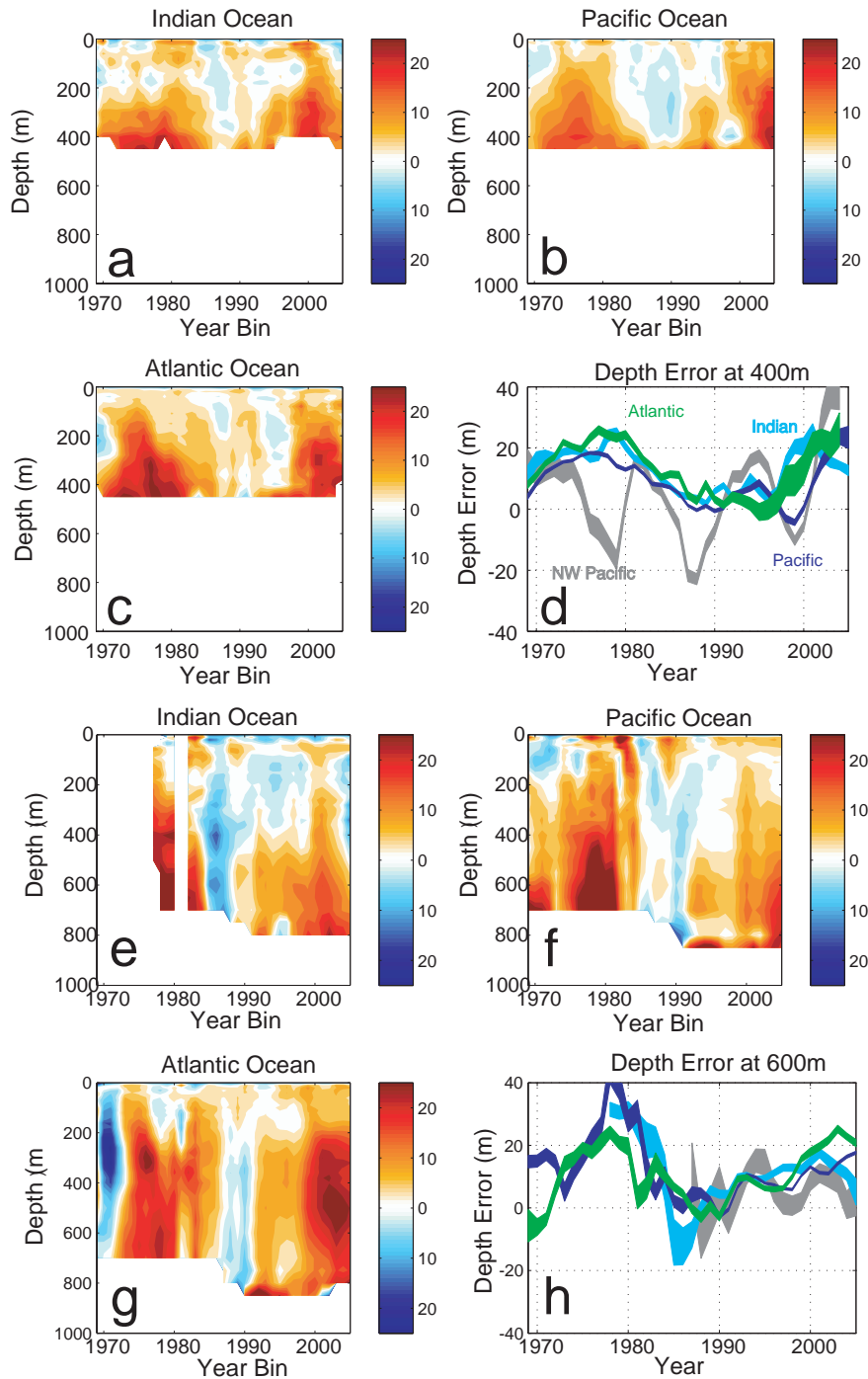


FIG. 6. Depth error time history for each ocean basin analyzed independently. Depth errors were averaged in 2 year bins and in each ocean basin. (a) – (c) for shallow XBTs in the Indian, Pacific and Atlantic Oceans; d) shallow XBT depth error at 400 m for each basin with the Indian, Pacific and Atlantic Oceans in cyan, blue and green respectively, with the northwest Pacific (longitudes  $< 155^{\circ}\text{E}$ , latitudes  $> 25^{\circ}\text{N}$ ) in gray; (e) – (g) for deep XBTs in the Indian, Pacific and Atlantic Oceans; h) deep

XBT depth error at 600 m for each basin with colours as in (d). In (d) and (h), curve thicknesses indicate the standard error of the estimate.

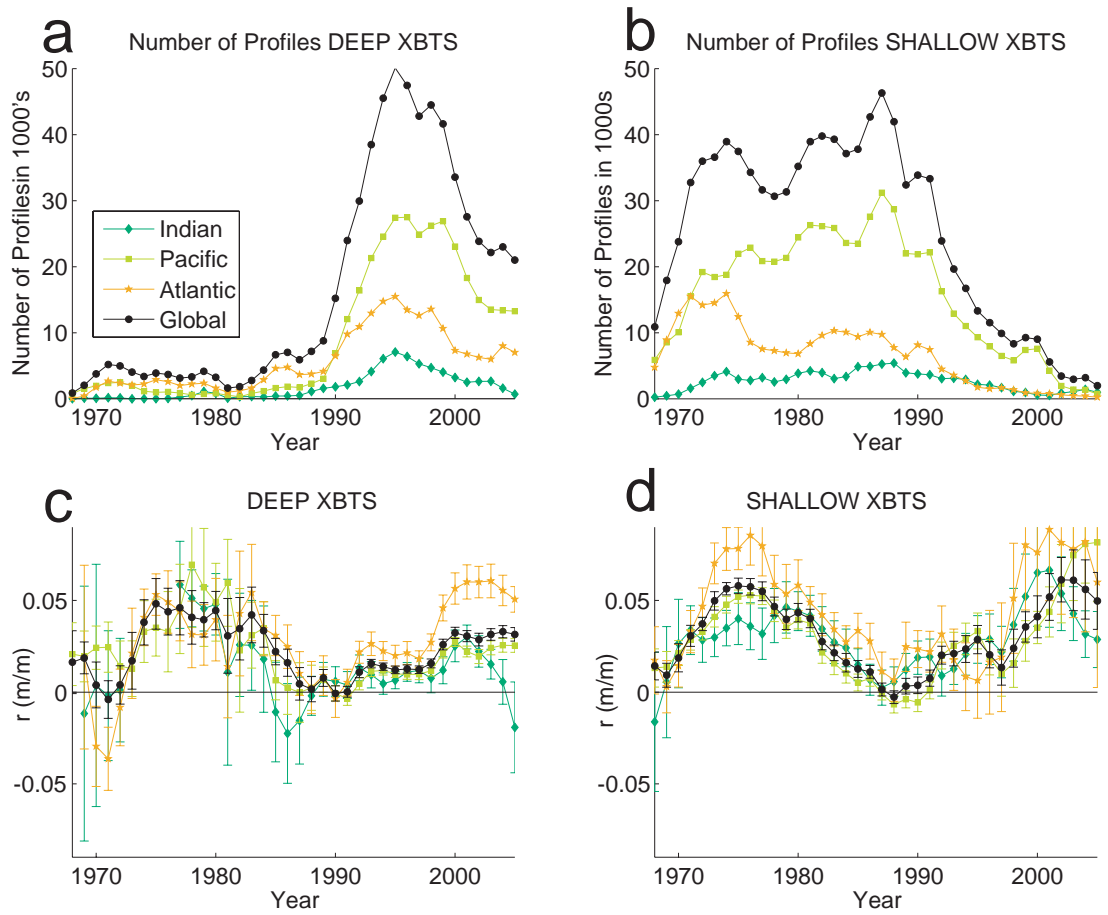


FIG. 7. Number of observations in 2 year bins for deep (a) and shallow (b) XBTs. XBT depth correction factor,  $r$ , averaged in overlapping 2 year bins for deep (c) and shallow (d) reaching profiles. Observation number (a, b) and fits (c, d) were analyzed in each ocean basin independently, as well as globally (see legend). Errors shown are 3 times the standard error, which encompasses 99.8% of the distribution (see text).

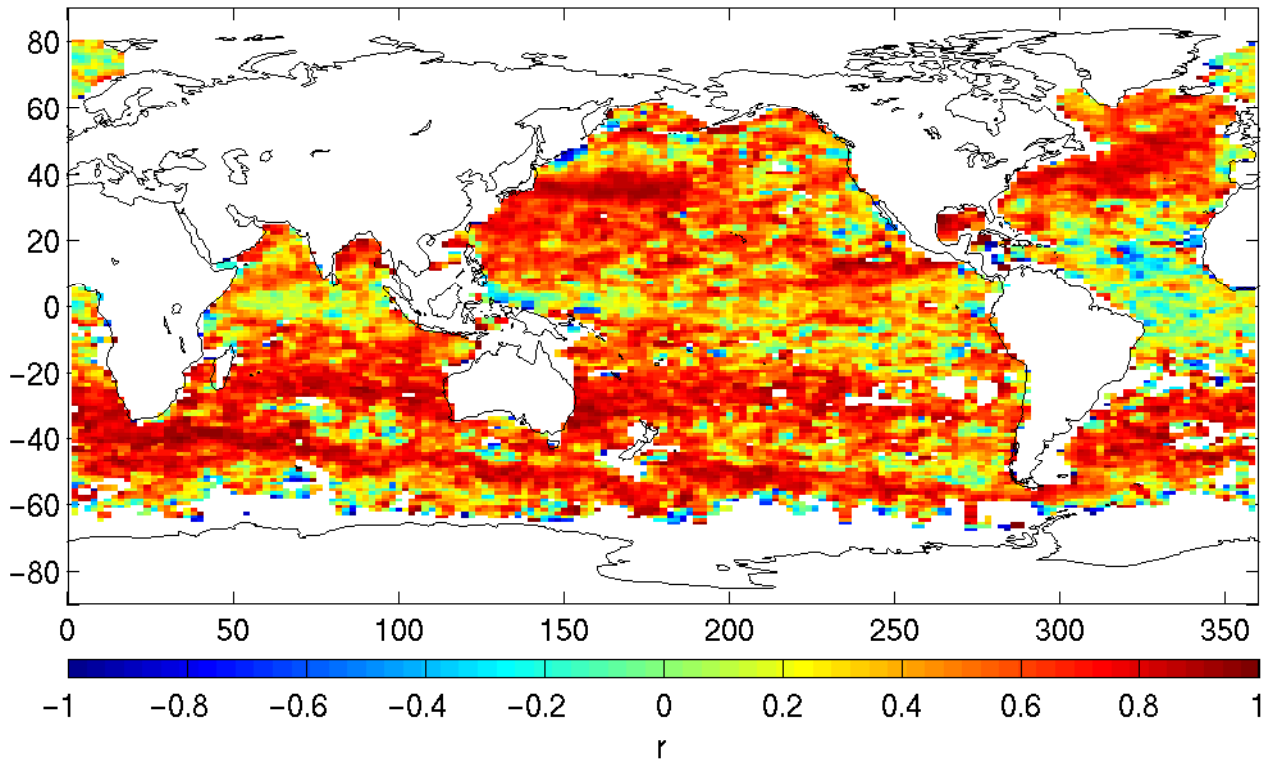


FIG. 8. Correlation coefficient between SSH and temperature anomaly at 400 m.



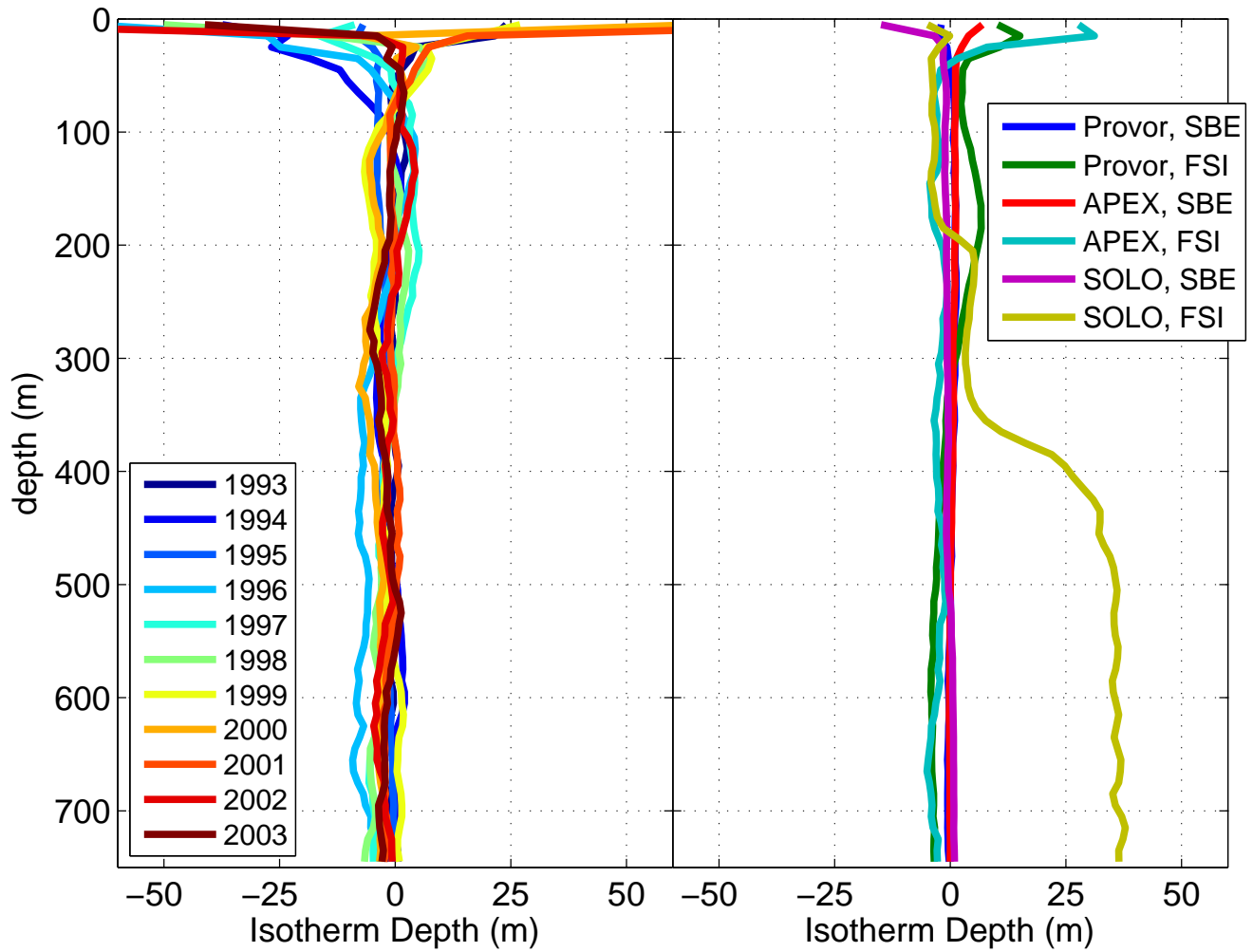


FIG. 9. Median depth error computed by comparing actual CTD profiles and their “pseudo-pairs” (left panel). Number of profiles ranges from 2000 to 6000 CTD profiles in a given year. Same for Argo float profiles by float type (right panel).

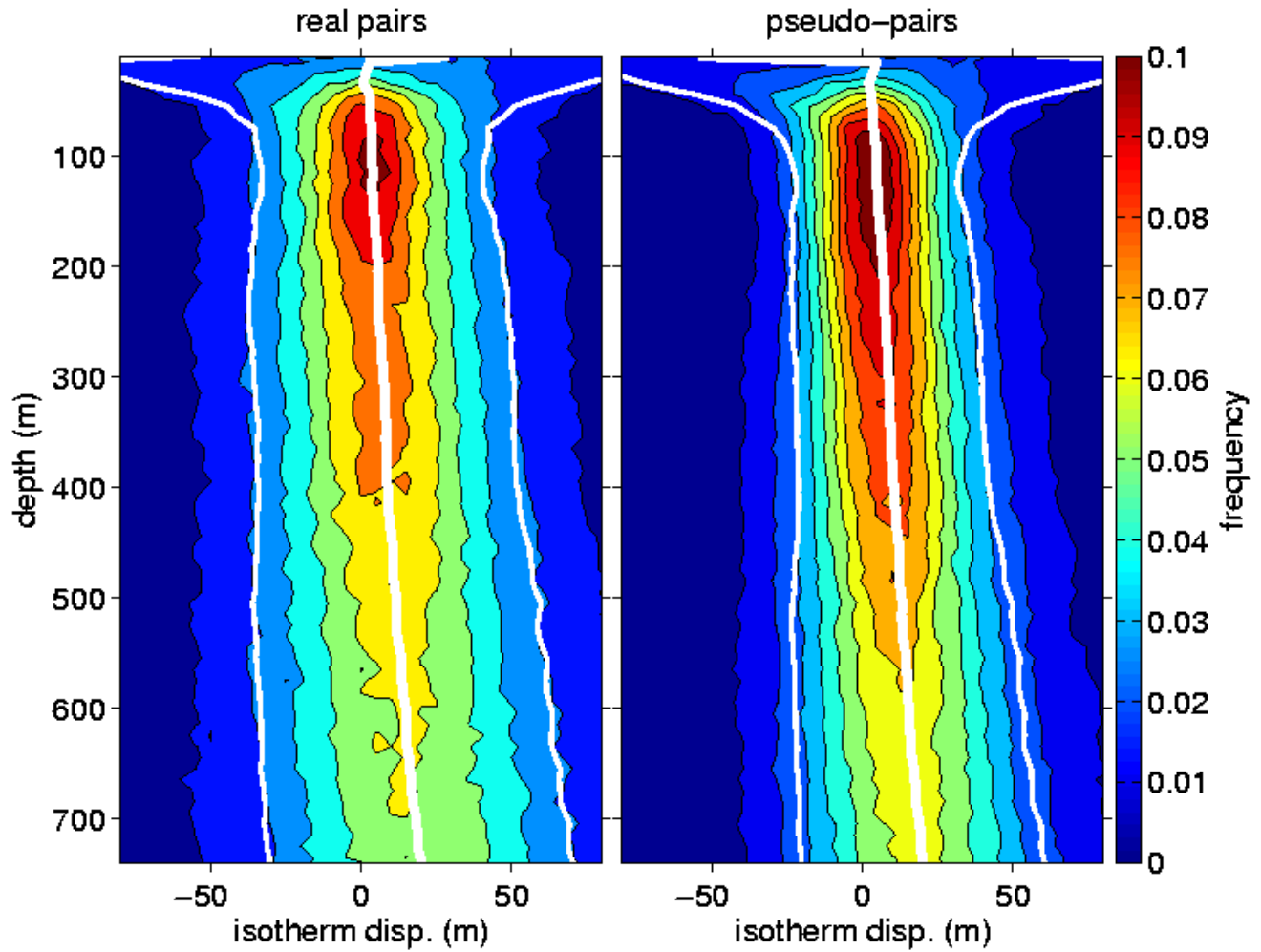


FIG. 10. Frequency distribution of difference in isotherm displacement v. depth for Sippican Deep blue XBT probe with H95 fall rate coefficients (WMO code, 052) compared with nearby Argo profiles (left panel) and pseudo pairs (right panel). Average is over the three-year period from Jan. 1, 2004, through Dec. 31, 2006. White lines show the median and one standard deviation.

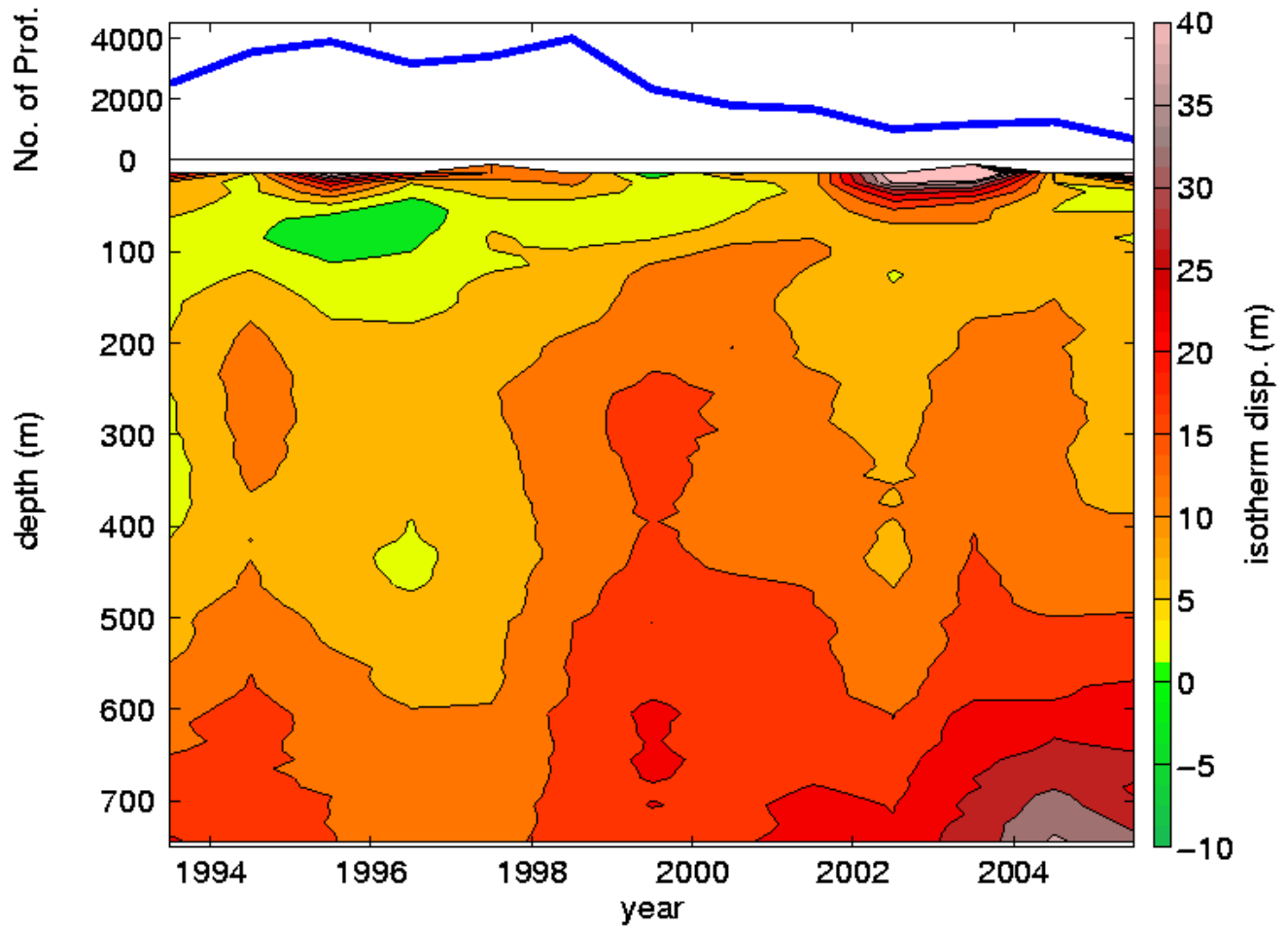


FIG. 11. Evolution of bias in for Sippican Deep blue XBT probe with old fall rate coefficients (WMO code, 051) using pseudo-pairs. The blue line shows the number of profiles used in a given year.

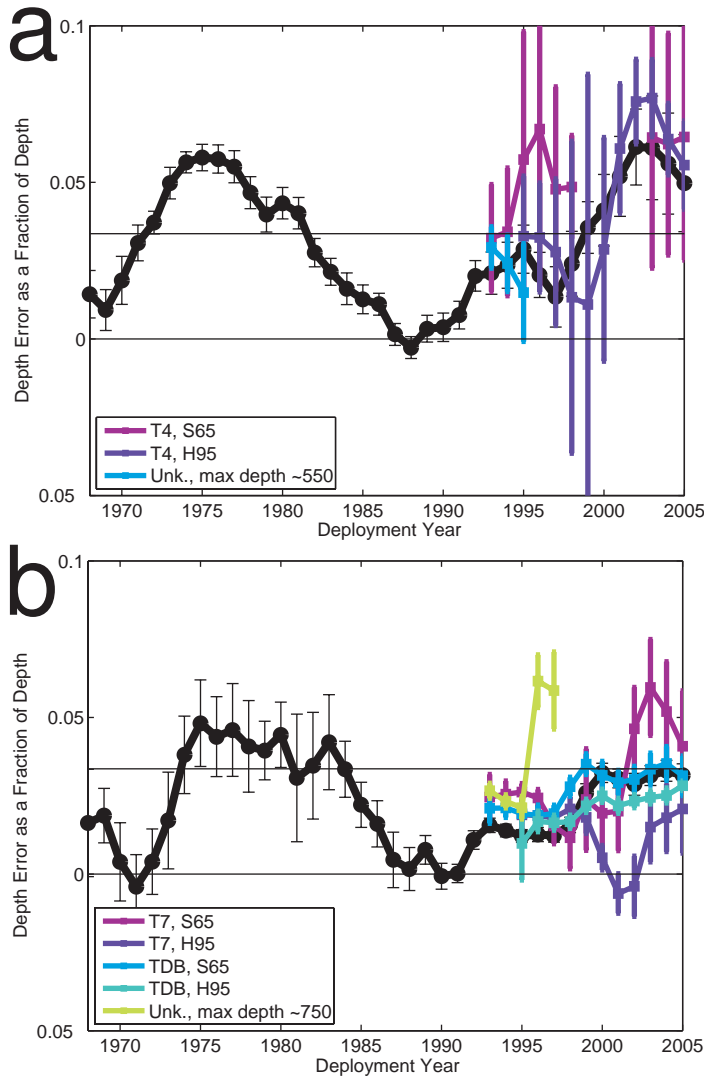


FIG. 12. In colours – the evolution of depth bias and its associated error (at 99% significance level) by probe type and depth equation used, as reported in Table 2. Results for shallow XBT profiles in (a) and for deep XBT profiles in (b). In the legend, T-7, T-4 and T-DB refer to Lockheed Martin Sippican’s probe models identified by the WMO number in the profile meta data in the archive, with H95 and S65 indicating the reported fall-rate equation used, where H95 refers to the Hanawa et al. (1995) recommendations and S65 indicates the manufacturer’s original estimate. The black line is the global bias estimated from EN3 with error bars as detailed in

Table 1. The two straight reference lines indicate fall-rates equal the H95 value (at zero) and the S65 value (at 0.0366).

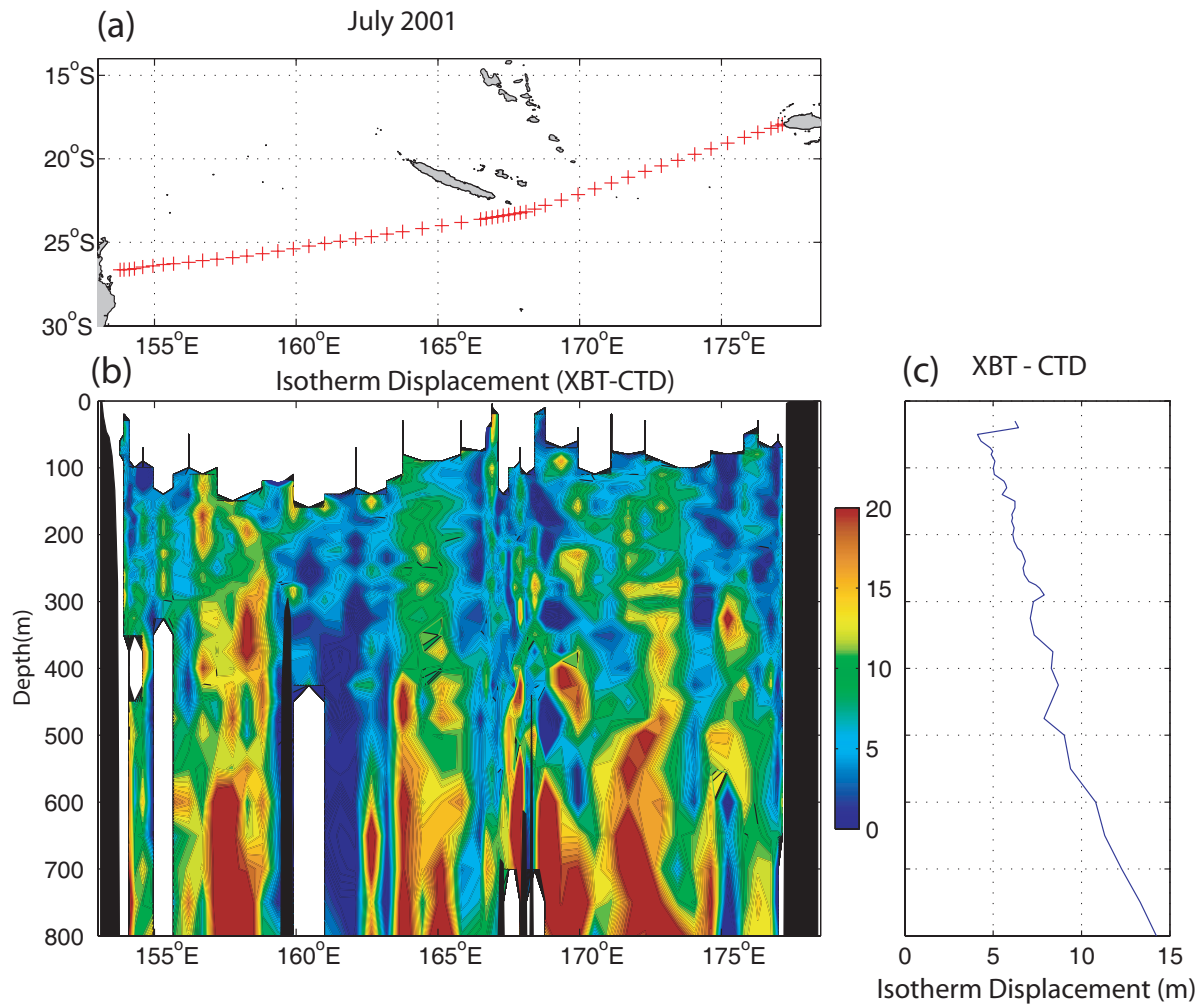


FIG. 13. During voyage of RV Franklin (July 2001) XBT casts were made concurrently at 52 CTD locations between Fiji and Brisbane. (a) Location of CTD stations, (b) Difference in isotherm depth between XBT and CTD temperature casts. Blank areas show mixed layer and location of topography. (c) Mean difference in isotherm depth for XBT and CTD casts.

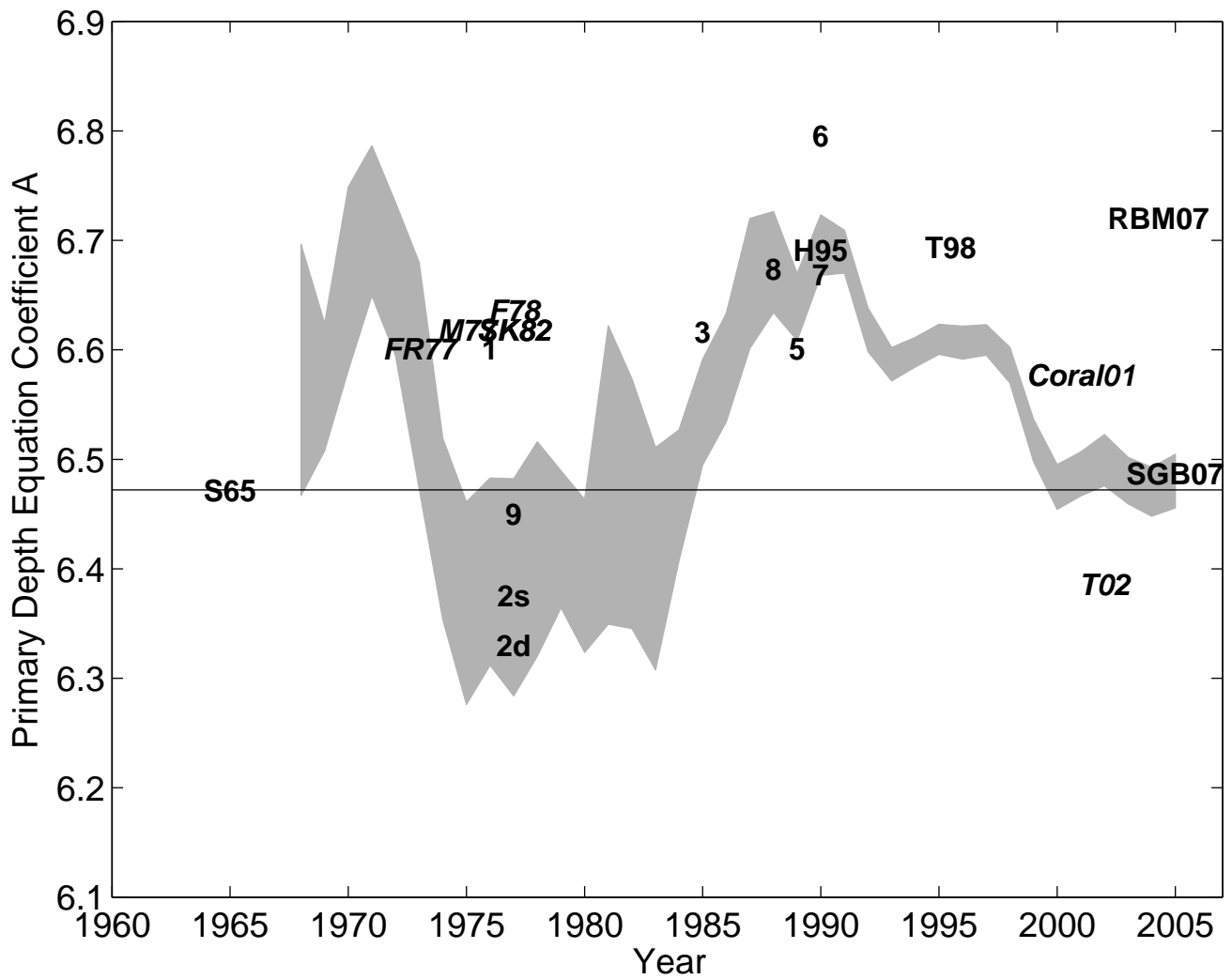


FIG. 14. Time history of the primary coefficient in the XBT fall-rate equation for deep XBTs as estimated from our analysis of the XBTs in the EN3 data set (grey line), estimates collated in H95's Table 1, and published results in Table 1 of this study. S65 refers to the manufacturer's recommended coefficient (also marked by the reference line), 'Coral01' refers to an estimate based on an XBT/CTD field comparison carried out in the Coral Sea in 2001. Text symbols are centered on the time and value they represent.

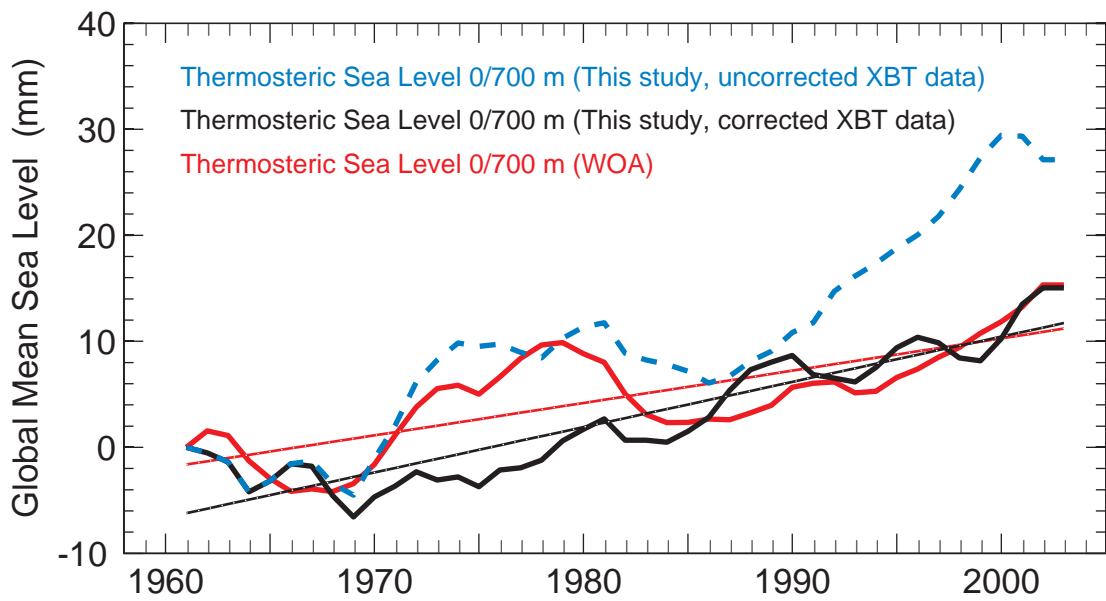


FIG. 15. Global mean thermosteric sea level estimates for the upper 700 m, relative to 1961. EN3 data, with (black) and without (blue) XBT profiles corrected for the fall-rate bias, referenced to an unbiased climatology (see text for details). WOA estimates (red) based on the data and reference climatology used in Antonov et al. (2005) and Levitus et al. (2005). Note that, in this latter case, both data and the climatology contain XBT bias. The thin straight lines are least-squares linear fits to the estimates. All time series were smoothed by a 3-year running mean.



TABLE 1. Diagnosed depth errors as a fraction of depth i.e.  $r = (\text{depth error})/\text{depth}$  based on the analysis of the EN3 archive where all profiles have been adjusted to the H95 fall-rates. Fractional depth errors for shallow XBTs are indicated by  $r_s$  and for deep XBTs by  $r_d$ . Errors shown encompass the 99<sup>th</sup> percentile based on a bootstrap analysis (see text).

Year	$r_s$	Error $r_s$	$r_d$	Error $r_d$
1968	0.014	0.008	0.016	0.017
1969	0.009	0.007	0.019	0.009
1970	0.019	0.008	0.004	0.013
1971	0.031	0.006	-0.004	0.010
1972	0.037	0.004	0.004	0.010
1973	0.050	0.005	0.017	0.015
1974	0.056	0.003	0.038	0.012
1975	0.058	0.004	0.048	0.014
1976	0.057	0.005	0.044	0.013
1977	0.055	0.005	0.046	0.015
1978	0.047	0.005	0.041	0.015
1979	0.040	0.006	0.039	0.009
1980	0.043	0.005	0.044	0.010
1981	0.040	0.005	0.031	0.020
1982	0.028	0.005	0.035	0.017
1983	0.021	0.004	0.042	0.015
1984	0.016	0.005	0.033	0.009
1985	0.013	0.005	0.022	0.007
1986	0.011	0.003	0.016	0.007
1987	0.001	0.003	0.005	0.009
1988	-0.003	0.004	0.002	0.007
1989	0.003	0.004	0.008	0.005
1990	0.004	0.005	-0.001	0.004
1991	0.008	0.004	0.000	0.003
1992	0.020	0.005	0.011	0.003
1993	0.021	0.007	0.016	0.002
1994	0.024	0.007	0.014	0.002
1995	0.029	0.008	0.012	0.002
1996	0.020	0.007	0.013	0.002
1997	0.013	0.010	0.012	0.002
1998	0.024	0.010	0.016	0.002
1999	0.036	0.008	0.026	0.003
2000	0.041	0.011	0.032	0.003
2001	0.052	0.013	0.031	0.003
2002	0.061	0.012	0.029	0.003
2003	0.061	0.017	0.031	0.003
2004	0.056	0.016	0.033	0.003
2005	0.050	0.016	0.032	0.004

TABLE 2. Diagnosed depth errors as a fraction of depth based on the altimetric pseudo-pair analysis. The data have been analyzed by WMO 1770 code number, which indicates whether the original or the H95 fall-rate equation was used to find depth.

<b>Probe</b>	<b>T-4 original</b>		<b>T-4 H95</b>		<b>T-7 original</b>		<b>T-7 H95</b>	
<b>WMO #</b>	<b>1</b>		<b>2</b>		<b>41</b>		<b>42</b>	
<b>Year</b>	<b>r</b>	<b>Error</b>	<b>r</b>	<b>Error</b>	<b>r</b>	<b>Error</b>	<b>r</b>	<b>Error</b>
1993	0.0322	0.0171	-	-	0.0246	0.0072	-	-
1994	0.0342	0.0204	-	-	0.0255	0.0042	-	-
1995	0.0573	0.0408	0.0328	0.0192	0.0262	0.0027	0.0189	0.0048
1996	0.0670	0.0501	0.0324	0.0174	0.0243	0.0027	0.0187	0.0033
1997	0.0478	0.0327	0.0277	0.0234	0.0154	0.0057	0.0180	0.003
1998	0.0485	0.0165	0.0133	0.0498	0.0116	0.0099	0.0208	0.0039
1999	0.0285	0.0297	0.0110	0.0735	0.0238	0.0162	0.0181	0.0051
2000	-	-	0.0286	0.0357	0.0194	0.0135	0.0052	0.0039
2001	-	-	0.0608	0.0207	0.0201	0.0126	-0.0062	0.0063
2002	-	-	0.0758	0.0135	0.0464	0.0132	-0.0039	0.0096
2003	0.0643	0.0417	0.0769	0.0123	0.0596	0.0153	0.0150	0.0111
2004	0.0622	0.0354	0.0638	0.0114	0.0519	0.0159	0.0180	0.0108
2005	0.0645	0.0393	0.0555	0.0141	0.0408	0.0177	0.0208	0.0141
2006	0.0787	0.0384	-	-	0.0245	0.0195	0.0284	0.0279
<b>Probe</b>	<b>T-DB original</b>		<b>T-DB H95</b>		<b>unknown, depth ~550 m</b>		<b>unknown, depth ~750 m</b>	
<b>WMO #</b>	<b>51</b>		<b>52</b>		<b>r</b>	<b>Error</b>	<b>r</b>	<b>Error</b>
<b>Year</b>	<b>r</b>	<b>Error</b>	<b>r</b>	<b>Error</b>	<b>r</b>	<b>Error</b>	<b>r</b>	<b>Error</b>
1993	0.0210	0.0048	-	-	0.0292	0.0066	0.0266	0.0024
1994	0.0211	0.0030	-	-	0.0241	0.009	0.0232	0.0021
1995	0.0193	0.0027	0.0098	0.0117	0.0148	0.0156	0.0212	0.0036
1996	0.0187	0.0033	0.0168	0.0033	-	-	0.0616	0.0084
1997	0.0193	0.0027	0.0164	0.0024	-	-	0.0586	0.0123
1998	0.0279	0.0030	0.0167	0.0021	-	-	-	-
1999	0.0351	0.0033	0.0218	0.0021	-	-	-	-
2000	0.0315	0.0045	0.0250	0.0021	-	-	-	-
2001	0.0292	0.0039	0.0218	0.0024	-	-	-	-
2002	0.0302	0.0042	0.0233	0.0021	-	-	-	-
2003	0.0335	0.0051	0.0245	0.0021	-	-	-	-
2004	0.0353	0.0054	0.0251	0.0024	-	-	-	-
2005	0.0314	0.0063	0.0282	0.0015	-	-	-	-
2006	-	-	0.0286	0.0024	-	-	-	-

TABLE 3. Summary of observed depth differences between Sippican XBTs and CTDs. Positive corrections mean that XBT depth readings are too deep. Fall-rate equations are shown for studies that fit these directly to the in situ data, where  $t$  is time in seconds since acquisition starts.

Reference and abbreviation	No. XBT	XBT type	Exp. Date	Location	Analysed Depth	Depth correction	Notes
Flierl and Robinson (1977) FR77	15	T-7	1973	central W Atlantic	0 - 800	2.1m (sd = 5.2) @ 250 m, -15m (sd = 3.9) @ 750 m	@ 17.5C, 3.9db, 6.2db(std dev), @ 10C, -14.4db, 4.1db(std dev) (xbt -ctd)
McDowell (1977) M77	47	T-7	1976	Sargasso Sea	0 - 750	-1.4 m (sd = 12.6) @ 250 m, -17m (sd = 9.1) @ 750 m	dZ = 0 m (std dev. = ~3) @ thermocline (28 - 20C)
Fedorov,et al (1978) F78	13	T-7	1977	central W Atlantic	0 - 750	8.8m @ 250 m, -19m @ 750 m	dZ = 5 m (std dev. = 3.8) @ thermocline (28 - 20C)
Seaver and Kuleshov (1982) SK82	51 52	T-7 T-7	1977 1977	central W Atlantic	0 - 750 0 - 750	-4.2m (sd = 13.8 ) @ 250 m, -17m (sd = 9.5 ) @ 750 m 3.5m (sd = 14.3) @ 250 m, -17m (sd = 8.6) @ 750 m	
Thadathil et al (1998) T98	~29	T-7	1994 - 97	Indian Ocean	0 - 750	$z = 6.694t - 0.00222t^2$	
Snowden et al, (2007) SGB07	370	T-7	2005	Subtropical North Pacific	0-800	$z = 6.4896t - 0.00191t^2$	Agreement across multiple acquisition systems
Reseghetti, Borghini and Manzella (2007) RBM07	230 1312	T-4 DB	9/2003- 10/2004	Western Mediterranean	0-460 0-950	$z = 6.570t - 0.00220t^2$ $z = 6.720t - 0.00235t^2$	Fall-rate range search limited to $6.600 \leq A \leq 6.850 \text{ms}^{-1}$